(Received 26 November 2025, Accepted 23 December 2025, Scheduled 25 January 2026)

Compact Four-Port Conformal MIMO Antenna with Asymmetric Ground for Wideband X-Band Applications

Velraju Prithivirajan[1], Kannan Vishnulakshmi[2], Palaniselvan Sundaravadivel[3], Muthu Manikam Anabarasu[4], Dhanushkodi Siva Sundara Raja[5], and Dhandapani Rajeshkumar[1,*]

[1] *Vel Tech Rangarajan Dr. Sagunthala R&D Institute of Science and Technology, Chennai, India*
[2] *Dr. N.G.P Institute of Technology, Coimbatore, India*
[3] *Saveetha Engineering College, Chennai, India*
[4] *Shanmuganathan Engineering College, Pudukkottai, India*
[5] *SACS MAVMM Engineering College, Madurai, India*

ABSTRACT: This paper presents a compact four-port conformal multiple-input multiple-output (MIMO) antenna designed on a 0.1-mm-thick transparent flexible polyimide substrate for wideband X-band wireless applications. Each antenna element is composed of an annular ring radiator and an asymmetric coplanar ground to achieve low mutual coupling and high diversity performance. The proposed MIMO antenna covers an impedance bandwidth of 7.9–14 GHz, with isolation greater than 20 dB and a maximum reflection coefficient of 32.5 dB at 10.5 GHz. The experimental results are in good agreement with the simulated ones in terms of reflection, transmission, and radiation characteristics. The measured gain ranges from 4.5 to 6 dBi, with stable radiation patterns across the operating band. The MIMO performance metrics, including envelope correlation coefficient (ECC $=$ 0.002), diversity gain ($\approx$ 10 dB), channel capacity loss ($<$ 0.3 bits/s/Hz), and total active reflection coefficient (TARC), confirm the suitability of the design for robust high-data-rate communication. Furthermore, the antenna maintains stable operation under various bending configurations, ensuring its potential for X-band conformal and wearable applications.

1. INTRODUCTION

Wearable and conformal antennas have gained significant attention over the past decade due to their critical role in emerging wireless technologies such as body area networks (BANs), telemedicine, military communications, and emergency response systems [1, 2]. As these applications require the seamless integration of electronic components with the human body or flexible platforms, antenna characteristics such as mechanical flexibility, compact size, and electromagnetic stability become essential. Among the various solutions, textile- and flexible-substrate-based antennas have demonstrated considerable potential, as they can be easily integrated into garments and wearable devices while maintaining satisfactory electrical performance [3–7].

A key challenge in wearable antenna design is ensuring user safety by maintaining a low specific absorption rate (SAR) and minimizing electromagnetic interaction with the human body. To address this issue, several techniques have been proposed, including electromagnetic bandgap (EBG) structures [8–10], artificial magnetic conductors (AMC) [11–13], and high-impedance surfaces (HIS) [14]. These surfaces function as electromagnetic shields by controlling the reflection phase and impedance characteristics, thereby reducing radiation leakage and energy absorption. However, such approaches often increase antenna size, fabrication complexity, and cost. Alternative solutions, such as cavity-backed configurations [15], can achieve unidirectional radiation but at the expense of increased thickness and structural rigidity, which limits their suitability for conformal and wearable applications.

In parallel, multiple-input multiple-output (MIMO) technology has emerged as an effective approach for enhancing channel capacity, improving link reliability, and mitigating multipath fading in dynamic body-centric environments [16–22]. However, implementing MIMO antennas on wearable or flexible platforms introduces additional challenges, particularly high mutual coupling between closely spaced antenna elements. Maintaining a low envelope correlation and high isolation within such constrained geometries is essential to ensure effective diversity performance. Several techniques — such as the incorporation of U-shaped or I-shaped ground stubs [18, 23], the use of metamaterial-inspired surfaces [19, 21], and the adoption of perpendicular or orthogonal element orientations [24–30, 45–47] — have been explored to mitigate mutual coupling. Although these methods improve isolation, they often require increased surface area, which conflicts with the compactness demanded by wearable and conformal systems.

Recent studies have reported notable advancements in compact and high-performance MIMO antenna designs, particularly for X-band, wideband, and conformal applications. Kulkarni et al. [32] proposed a dual-circularly polarized quad-port X-band MIMO antenna that effectively suppresses mutual coupling through orthogonal element placement and optimized radiator geometry, demonstrating the benefits of polarization

* Corresponding author: Dhandapani Rajeshkumar (sdrk87@gmail.com).

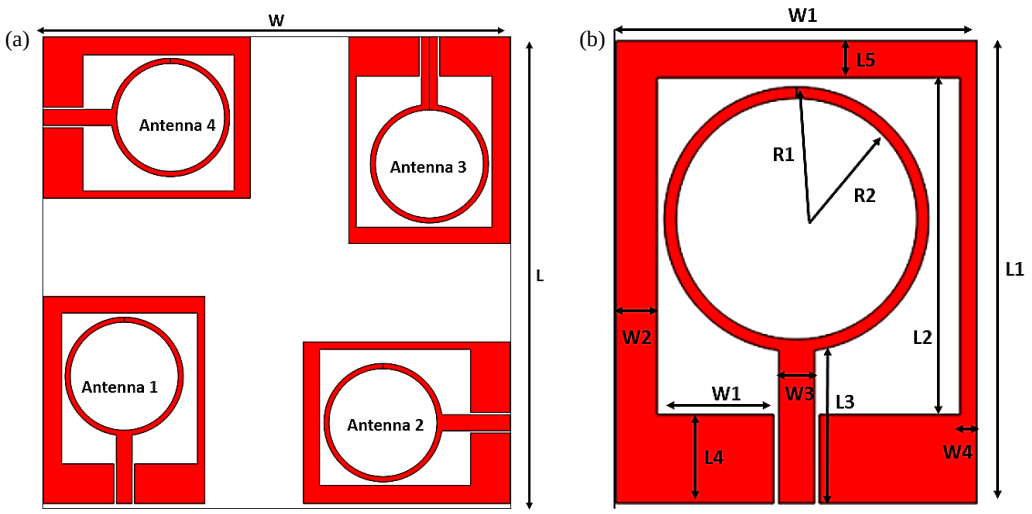

FIGURE 1. (a) Structure of proposed MIMO antenna, (b) structure and dimension of Antenna 1.

diversity at higher frequencies. Agarwal and Rafique [46] introduced a super-wideband circular ring fractal antenna with a high bandwidth dimension ratio (BDR), illustrating how iterative fractal perturbations can significantly enhance bandwidth while maintaining a compact footprint. Saurabh et al. [48] presented a compact wideband four-element MIMO antenna aimed at achieving high isolation within a limited footprint, where the design emphasizes structural symmetry and optimized element spacing to suppress mutual coupling without relying on complex decoupling networks. The proposed configuration demonstrates that a careful geometrical arrangement of radiating elements can simultaneously support wide impedance bandwidth and effective isolation, making it suitable for compact wireless terminals. In contrast, Jhunjhunwala et al. [49] focused on a four-port flexible ultra-wideband (UWB) MIMO antenna tailored for wearable applications, where both mechanical flexibility and electromagnetic performance are critical. Their design employs a flexible substrate and isolation-enhancement techniques to mitigate coupling effects caused by close element proximity and body-centric operation. Together, these works highlight two complementary research directions in MIMO antenna development: achieving high isolation in compact rigid platforms for conventional wireless devices, and ensuring stable, low-coupling performance in flexible UWB MIMO systems intended for wearable and body-area network applications.

In this context, the present work introduces a compact four-port conformal MIMO antenna printed on a 0.1-mm-thick transparent polyimide substrate. Each antenna element consists of an annular ring radiator combined with an asymmetric coplanar ground structure, optimized to achieve wideband impedance matching and low inter-port coupling. The antenna operates efficiently over the 7.9–14 GHz frequency range, covering the X-band spectrum with isolation better than 20 dB. The proposed configuration exhibits excellent MIMO performance, including a low envelope correlation coefficient (ECC) of 0.002, a diversity gain of approximately 10 dB, and a channel capacity loss below 0.3 bits/s/Hz. Furthermore, the antenna maintains stable electromagnetic performance under various bending conditions, confirming its suitability for flexible, wearable, and conformal wireless applications.

2. ANTENNA DESIGN AND ANALYSIS

Figure 1 illustrates the structural configuration of the proposed four-port conformal MIMO antenna system. The overall antenna geometry, shown in Fig. 1(a), is realized on a compact flexible substrate with dimensions $L \times W = 65\,\text{mm} \times 65\,\text{mm}$, where four identical radiating elements (Antenna 1–Antenna 4) are positioned at the corners of the substrate in an orthogonal orientation. This orthogonal arrangement provides both polarization and spatial diversity and simultaneously reduces mutual coupling among the ports without the need for additional decoupling networks. The coplanar configuration ensures that all radiating elements and ground planes are printed on the same side of the substrate, which simplifies fabrication and preserves conformal flexibility.

Figure 1(b) presents the structural layout and dimensional details of a single antenna element (Antenna 1). The antenna employs an annular ring radiator as the primary radiating element. The ring is characterized by an outer radius R_1 and an inner radius R_2, which jointly govern the resonant frequency and impedance bandwidth. Excitation is provided through a rectangular 50-Ω microstrip feed line with dimensions $L_3 \times W_3$, enabling efficient power transfer and impedance matching across the 7.9–14 GHz operating band. The ground plane is intentionally designed with asymmetry, comprising unequal left (W_2) and right (W_4) ground arms. This asymmetric coplanar ground structure modifies the surface current distribution and introduces multiple resonant modes, thereby enhancing impedance bandwidth and improving reflection characteristics. Furthermore, the ground extensions L_4 and L_5 are used to fine-tune the reactive fields in the vicinity of the feed and radiating ring, resulting in optimized return loss and balanced radiation performance. The upper rectangular slot region with dimensions $L_1 \times W_1$ encloses the ring radiator and functions as an impedance transformer, contributing to stable current distribution across the antenna structure.

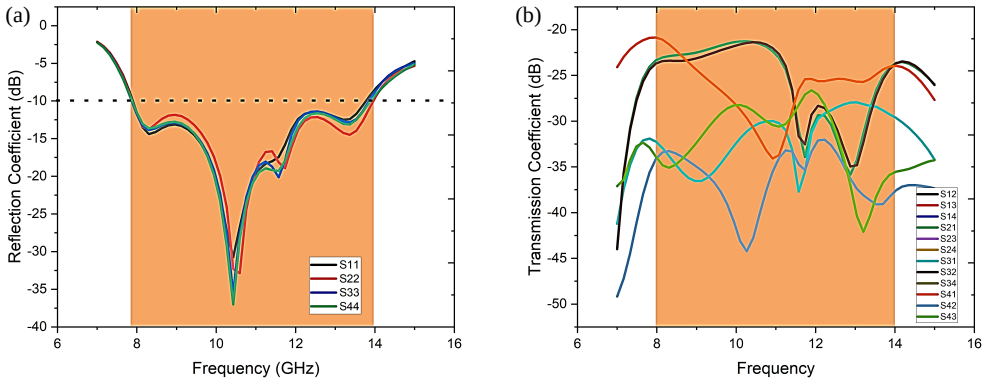

FIGURE 2. Simulated S-parameters of the MIMO antenna. (a) Reflection coefficient, (b) transmission coefficient.

The detailed dimensions of the proposed MIMO antenna system are listed in Table 1.

TABLE 1. Various design parameters of the proposed antenna.

Parameter	Value (mm)	Parameter	Value (mm)
L	65	W	65
L_1	28.8225	W_1	22.5
L_2	21	W_2	2.55
L_3	9.5271	W_3	2.25
L_4	5.5225	W_4	1.05
R_1	8.2	R_2	7.5

Figure 2 illustrates the simulated S-parameters of the proposed four-port MIMO antenna, highlighting both the reflection and transmission characteristics over the frequency range of 7–14 GHz. As shown in Fig. 2(a), the reflection coefficients (S_{11}, S_{22}, S_{33}, and S_{44}) indicate excellent impedance matching for all four antenna elements, with return losses better than -10 dB across the 7.9–14 GHz operating band and a minimum reflection coefficient of approximately -32.5 dB at 10.5 GHz. This behaviour confirms that each element resonates efficiently and maintains a stable input impedance over a wide bandwidth, fully covering the X-band spectrum.

Figure 2(b) presents the transmission coefficients (S_{12}, S_{13}, S_{14}, S_{23}, S_{24}, S_{34}, and their symmetric counterparts), which characterize the isolation between antenna ports. The results demonstrate that the mutual coupling between any two ports remains below -20 dB throughout the operating frequency range, indicating excellent inter-port isolation. This high isolation is primarily attributed to the orthogonal arrangement of the antenna elements and the asymmetric coplanar ground structure, which together suppress surface current coupling. Such performance ensures low signal correlation among the ports, making the proposed antenna well-suited for MIMO-based high-data-rate X-band communication systems where wide bandwidth and strong isolation are critical for reliable diversity operation.

3. PARAMETRIC STUDY

This section investigates the effects of key design parameters on the performance of the proposed MIMO antenna. Although several geometrical parameters influence the antenna characteristics, only the primary parameters — namely W_2, L_4, and W_4 — are considered for brevity. As shown in Fig. 3(a), the influence of the ground-plane width (W_2) on the impedance response is examined. When W_2 is varied from 1.05 mm to 2.55 mm with a uniform step size; noticeable changes in impedance matching are observed across the desired operating band. Specifically, a reduction in W_2 leads to degraded reflection characteristics, indicating poorer impedance matching.

Similarly, the bottom ground-plane length (L_4) is varied from 5.0225 mm to 6.5225 mm, and the corresponding effects on antenna performance are analyzed, as illustrated in Fig. 3(b). Variations in L_4 result in a shift of the resonant frequency toward the lower or higher ends of the spectrum, demonstrating that L_4 plays a critical role in determining the operating frequency. In addition, changes in the left-side ground-plane width (W_4) significantly affect the impedance matching of the antenna, as depicted in Fig. 3(c). These results confirm that careful optimization of the ground-plane dimensions is essential for achieving wideband operation and stable impedance characteristics in the proposed MIMO antenna.

4. SURFACE CURRENTS

Figure 4 illustrates the simulated surface current distribution of the proposed MIMO antenna when Antenna 1 is excited at three representative resonant frequencies — 8.5 GHz, 9.5 GHz, and 12 GHz — while the remaining ports are terminated with 50-Ω loads. At 8.5 GHz, as shown in Fig. 4(a), strong current concentrations are observed along the right edge of the asymmetric ground plane and partially over the annular ring radiator, indicating that both the feed line and the adjacent ground structure contribute to the lower-frequency resonance. When the excitation frequency increases to 9.5 GHz, as depicted in Fig. 4(b), the surface current is predominantly confined around the annular ring, exhibiting a more uniform and balanced distribution. This behaviour supports efficient radiation and improved impedance matching in the mid-band region. At 12 GHz, shown in Fig. 4(c), the peak current density shifts toward the upper and right edges of the ground plane, suggesting the excitation of higher-order resonant modes that contribute to bandwidth extension at higher frequencies.

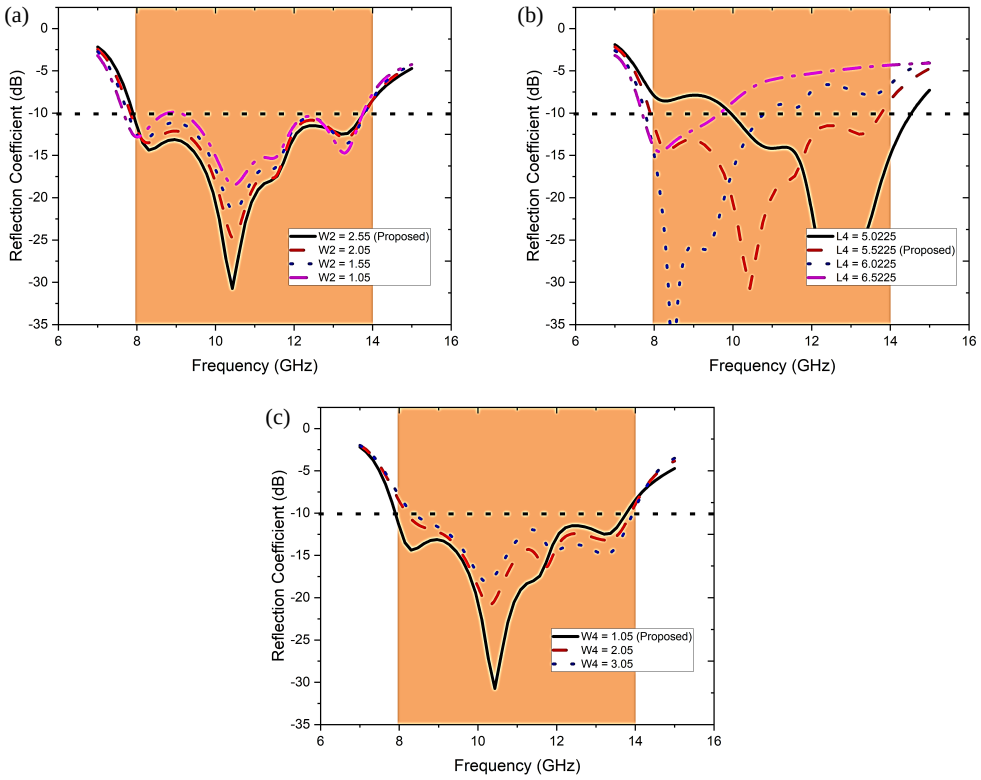

FIGURE 3. Parametric analysis when changing (a) W_2, (b) L_4, (c) W_4.

Notably, a negligible induced current is observed on the non-excited antenna elements at all three frequencies, confirming excellent port isolation (greater than 20 dB) and low mutual coupling within the MIMO configuration. This behaviour validates the effectiveness of the asymmetric coplanar ground structure and orthogonal element orientation in controlling surface current flow, thereby enhancing MIMO performance while maintaining stable radiation characteristics across the wide 7.9–14 GHz operating band.

5. MEASURED RESULTS AND DISCUSSIONS

The proposed four-element conformal MIMO antenna was fabricated, and all antenna parameters were experimentally evaluated. Figs. 5(a) and 5(b) present the front and back views of the fabricated prototype. Each antenna element in the MIMO configuration is excited using a 50-Ω SMA connector, and during measurements, the non-excited ports are terminated with 50-Ω loads to ensure proper impedance matching and accurate characterization.

Figures 5 and 6 collectively illustrate the fabricated prototype and the measured S-parameter validation of the proposed four-port conformal MIMO antenna. Fig. 5 presents the front and rear views of the fabricated prototype. The antenna is realized on a 0.1-mm-thick transparent flexible polyimide substrate, providing both mechanical flexibility and structural stability for conformal applications. The front view, shown in Fig. 5(a), clearly depicts the four annular ring radiating elements arranged in an orthogonal configuration, with each element excited through a 50-Ω SMA connector to ensure proper impedance matching. The rear view, shown in Fig. 5(b), displays the ground plane and copper traces, confirming accurate fabrication and precise alignment of the feed lines. This configuration minimizes parasitic coupling while preserving a compact form factor suitable for wearable and curved-surface installations. Fig. 6 compares the measured reflection and transmission coefficients of the antenna to validate its simulated performance. As illustrated in Fig. 6(a), the measured reflection coefficients (S_{11}, S_{22}, S_{33}, and S_{44}) demonstrate good impedance matching for all four antenna elements over the 7.9–14 GHz frequency range, with a minimum return loss exceeding -30 dB near 10.5 GHz, in close agreement with the simulated results. Fig. 6(b) shows the measured transmission coefficients between antenna ports (S_{12}, S_{13}, S_{14}, and related parameters), indicating that the inter-port isolation remains better than -20 dB across the operating band. The strong correlation between the simulated and measured responses confirms the accuracy of the design methodology, the structural symmetry of the antenna, and the effectiveness of the asymmetric ground structure and orthogonal element arrangement in achieving high isolation. These results demonstrate that the proposed antenna provides a wide impedance bandwidth, strong inter-element isolation, and consistent performance, making it a reliable candidate for wideband X-band MIMO and conformal communication systems. Figs. 7 and 8 display simulated and measured far-field patterns of Antennas 1 and 2 at three distinct frequencies, respectively.

The simulated and measured gains of Antennas 1 and 2 are presented in Fig. 9(a). The results indicate that each antenna maintains a stable gain ranging from 4.5 dBi to 6 dBi across the

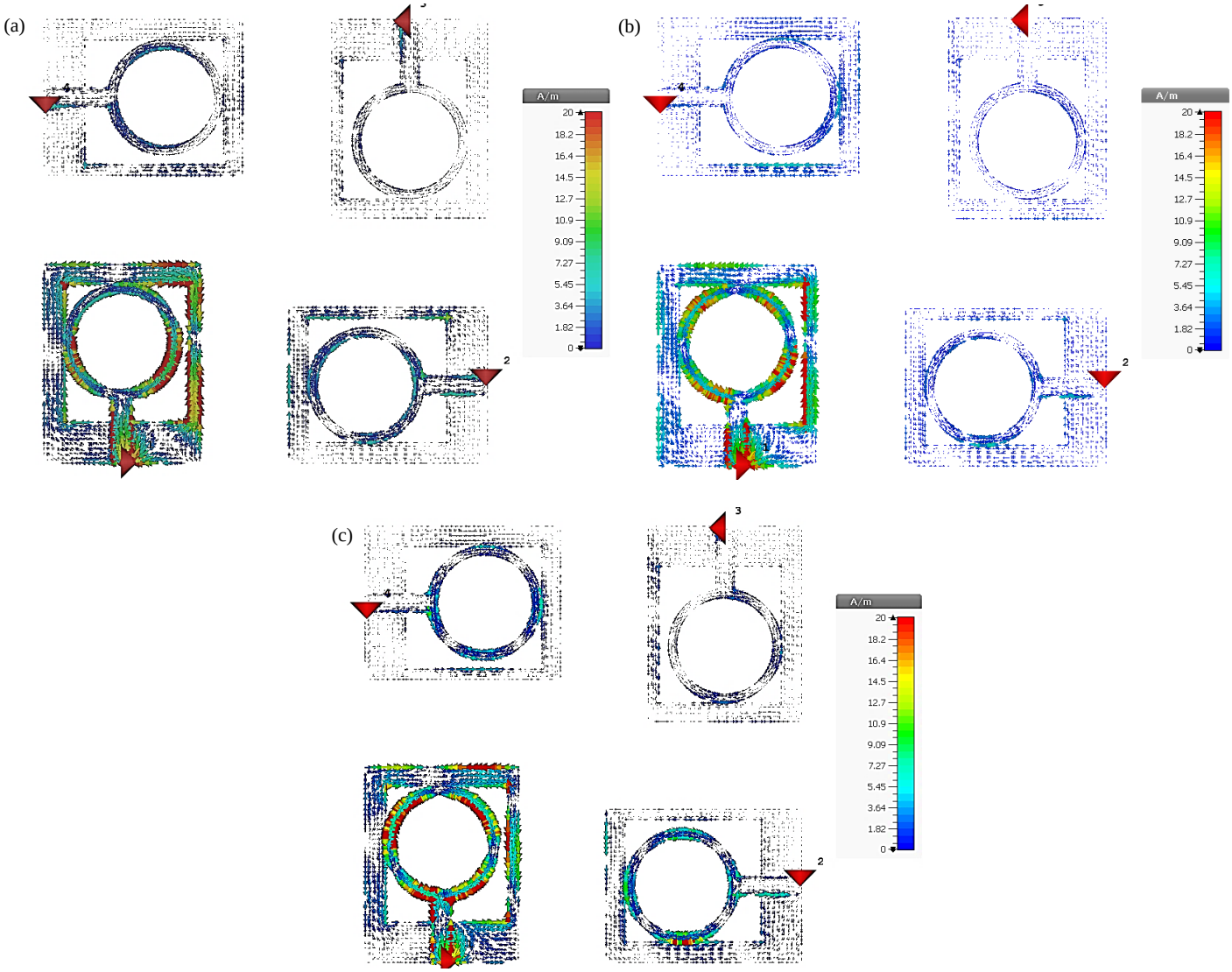

FIGURE 4. Surface currents when 1 is excited at (a) 8.5 GHz, (b) 9.5 GHz, (c) 12 GHz.

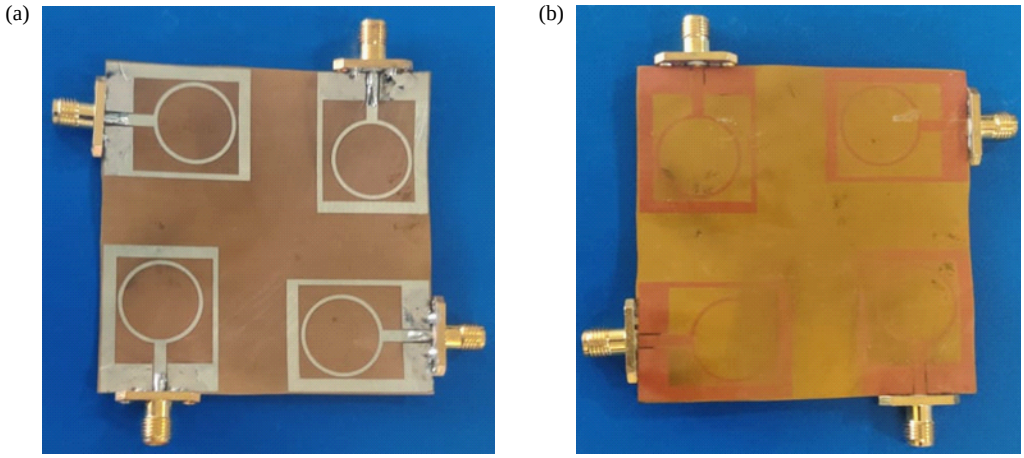

FIGURE 5. Manufactured prototype. (a) Front view, (b) rear view.

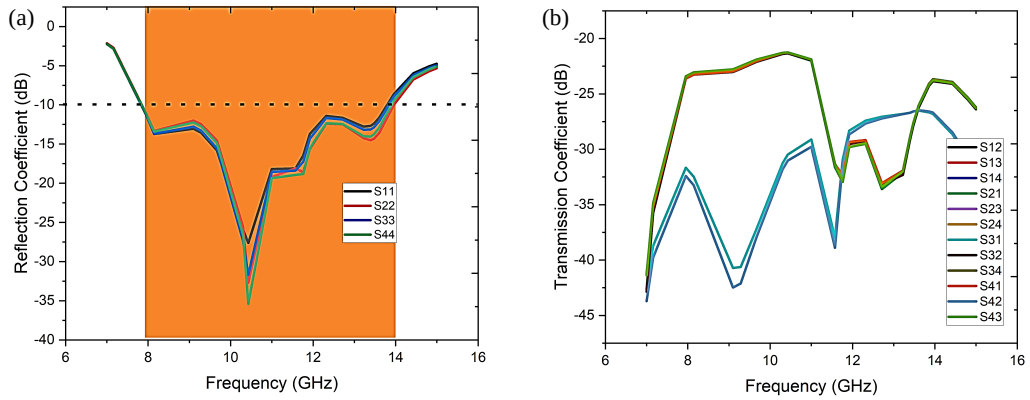

FIGURE 6. Measured (a) reflection coefficient, (b) transmission coefficient.

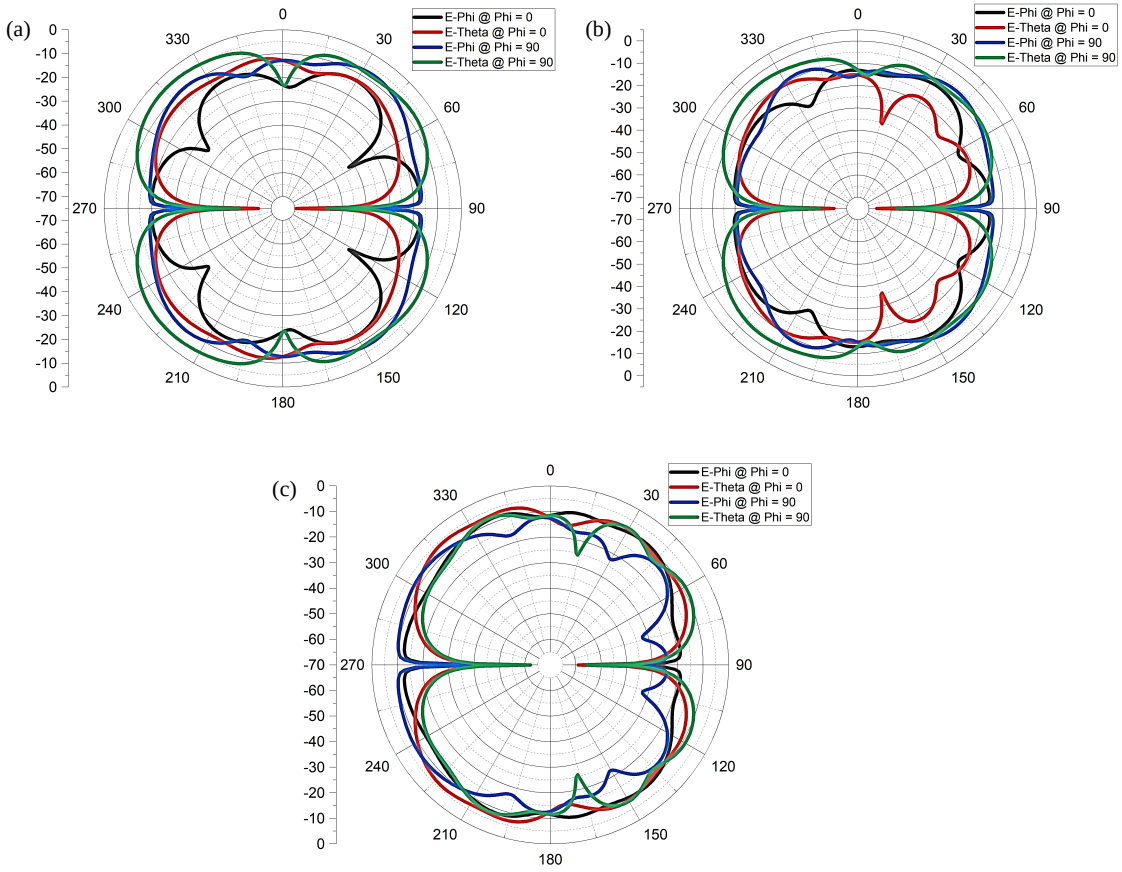

FIGURE 7. Two-dimensional radiation pattern of antenna 1 at (a) 8.5 GHz, (b) 9.5 GHz, (c) 12.5 GHz.

entire operating frequency band. This level of gain is adequate for the proposed MIMO antenna system and confirms its suitability for X-band wireless applications.

Figure 9(b) illustrates the simulated radiation efficiency of the four antenna elements (Antennas 1–4) over the 8–14 GHz frequency range, as indicated by the shaded region. Each antenna exhibits frequency-dependent efficiency variations, characterized by distinct peaks and minor dips across the band. Notably, Antenna 3 demonstrates comparatively higher efficiency in the 9–10 GHz and 12–13.5 GHz ranges, while Antennas 2 and 4 maintain relatively stable efficiency throughout the operating spectrum. These variations can be attributed to differences in impedance matching, radiation behavior, and inter-element coupling effects. Furthermore, the observed efficiency degradation outside the shaded region (below 8 GHz and above 14 GHz) indicates reduced operational performance beyond the intended bandwidth. The presence of multiple resonant features within the operating range confirms the wideband nature of the proposed antenna system. However, for practical deployment, further validation through measured efficiency data is necessary to corroborate the simulated results.

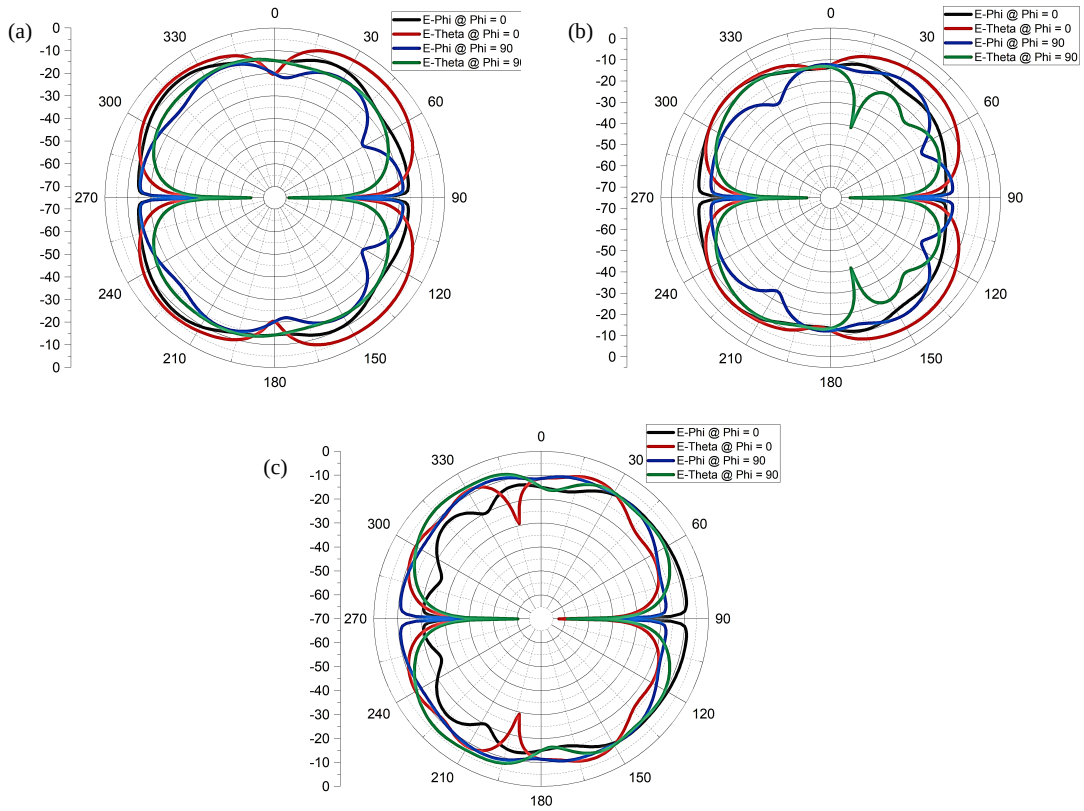

FIGURE 8. Two-dimensional radiation pattern of antenna 2 at (a) 8.5 GHz, (b) 9.5 GHz, (c) 12.5 GHz.

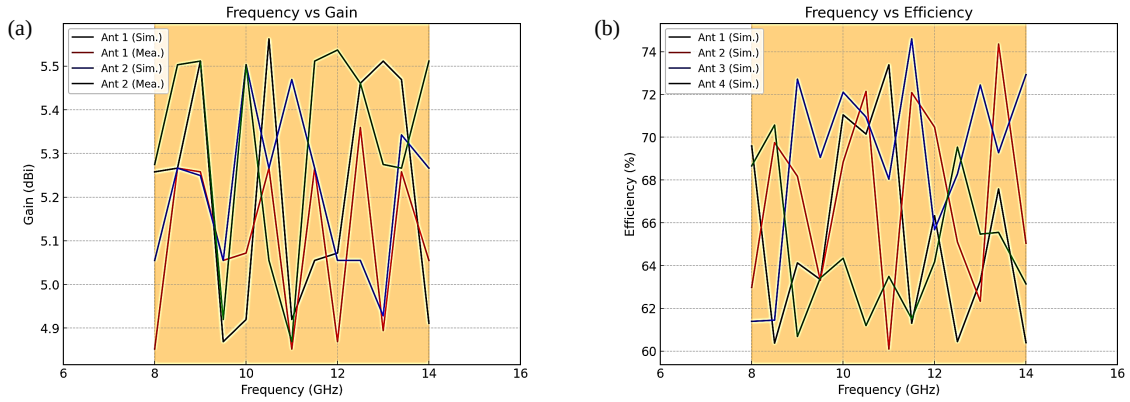

FIGURE 9. (a) Gain of Antenna 1 and Antenna 2, (b) efficiency of the proposed antenna.

6. MIMO PARAMETERS

It is essential to evaluate key MIMO performance metrics to assess the robustness of the proposed antenna system. Fig. 10(a) presents the envelope correlation coefficient (ECC) between the antenna elements, calculated from the measured S-parameters. The ECC provides insight into the degree of correlation and mutual independence among the antenna elements. For an ideal MIMO system, the ECC is zero; however, in practical implementations, values below 0.1 are considered acceptable. As shown in Fig. 10(a), the proposed antenna exhibits an exceptionally low ECC of approximately 0.002 across the operating band, indicating excellent isolation and strong MIMO performance. Diversity gain (DG) is another important parameter for evaluating the effectiveness of a MIMO antenna system. Fig. 10(b) illustrates the diversity gain of the proposed antenna, which remains very close to the ideal value of 10 dB across the operating frequency range. These results confirm the capability of the proposed MIMO antenna to provide reliable diversity performance and enhanced link quality for wideband X-band applications.

The channel capacity loss (CCL) of the proposed antenna is evaluated using (1) and (2). CCL quantifies the reduction in data transmission capacity resulting from correlation and mutual coupling among the antenna elements. In MIMO systems, CCL is commonly derived from the envelope correlation coefficients (ECCs), and values below 0.4 bits/s/Hz are gener-

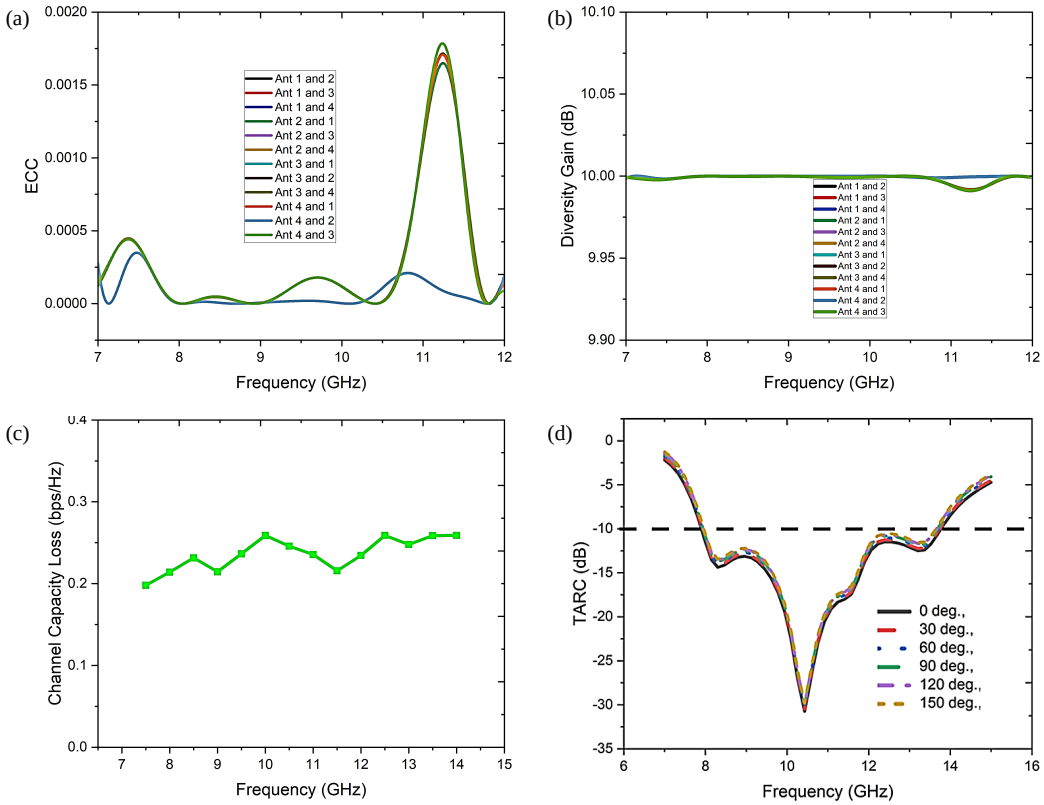

FIGURE 10. MIMO parameters, (a) ECC, (b) diversity gain, (c) CCL, (d) TARC.

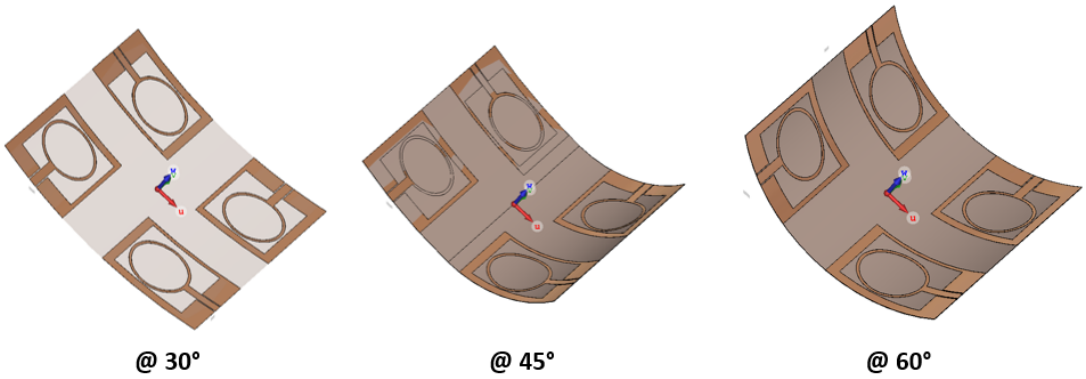

FIGURE 11. Various bending configurations of the proposed antenna.

ally considered acceptable for practical applications. As shown in Fig. 10(c), the calculated CCL of the proposed antenna remains below 0.3 bits/s/Hz across the operating frequency band, thereby confirming its suitability for efficient high-capacity MIMO communication.

$$\text{Channel Loss (CL)} = -\log_2 \det(A^r) \tag{1}$$

$$A^r = \begin{bmatrix} ECC_{ii} & \cdots & ECC_{ij} \\ \vdots & \ddots & \vdots \\ ECC_{ji} & \cdots & ECC_{jj} \end{bmatrix} \tag{2}$$

where,

$$ECC_{ii} = 1 - \left(\left(S_{ii}^2\right) + \left(S_{ij}^2\right)\right) \tag{3}$$

$$ECC_{ij} = -\left(S_{ii}^* S_{ij} + S_{ji}^* S_{jj}\right) \quad \text{for } i, j = 1, 2, \ldots, 4 \tag{4}$$

The total active reflection coefficient (TARC) of the proposed MIMO antenna system is evaluated by varying the excitation phase angles of all antenna elements except the antenna under test. In this analysis, the phase of Antenna 1 is held constant, while the phases of Antennas 2, 3, and 4 are varied from 0° to 150° , and the corresponding TARC responses are plotted, as shown in Fig. 10(d). The results indicate that the effective bandwidth of Antenna 1 remains largely unaffected by changes in the phase angles of the other radiating elements. This behavior demonstrates the robustness of the proposed MIMO configuration under different excitation conditions, confirming that the antenna is a strong candidate for X-band wireless applications.

TABLE 2. Performance comparison of the proposed antenna with the literature.

Reference No.	Single Antenna Size (mm^2)	Frequency (GHz)	Spectrums (GHz)	Gain (dBi)	Electrical Dimension of the Antenna (mm^2)
[31]	30×30	5.5	4.8–5.99	2.5	$0.043\lambda \times 0.043\lambda$
[32]	36×27	7.90–9.59	7.90–9.59	3.5	$0.0748\lambda \times 0.0561\lambda$
[33]	28×32	5.8 and 8	—	4.5 and 7.38	$0.042\lambda \times 0.0488\lambda$
[34]	50×50	1.28 and 2.43	1.198–1.345 and 2.395–2.484	NA	$0.018\lambda \times 0.018\lambda$
[35]	20×15	3.9	3.3–7.35	2.25	$0.0205\lambda \times 0.015\lambda$
[36]	25×25	4.175, 9.05	3.34–5.01, 8.9–9.2	4	$0.612\lambda \times 0.612\lambda$
[37]	62×40	3.9 and 4.9	—	3 and 3.5	$0.0636\lambda \times 0.041\lambda$
[38]	29×29	2.4 and 5.5	2.25–2.45 and 5.2–5.75	1 and 0.6	$0.018\lambda \times 0.018\lambda$
[39]	29×40	3.5 and 5.2	3.35–3.9 and 4.8–6	NA	$0.026\lambda \times 0.036\lambda$
[40]	20×40	2.45 and 5.8	2.37–2.42 & 5.7–5.84	0.4 & 1.6	$0.012\lambda \times 0.0252\lambda$
[41]	32×15	3.5, 5.8, and 7.5	—	1.2, 2.8, and 4	$0.025\lambda \times 0.011\lambda$
[42]	85.5×85.5	1.575 and 2.45	1.455–1.965 and 2.26–2.57	1.08 and 1.97	$0.035\lambda \times 0.035\lambda$
[43]	35×50	2.5 and 5.5	2.15–3.03 and 5–6.05	2.5 and 2.75	$0.023\lambda \times 0.032\lambda$
[44]	60×50	2.45 and 5.8	2.4–2.5 and 5.725–5.875	2.2 and 2.8	$0.0386\lambda \times 0.0322\lambda$
Proposed Work	22.5×28.8225	11	7.9–13.5	4.8	$0.023\lambda \times 0.0152\lambda$

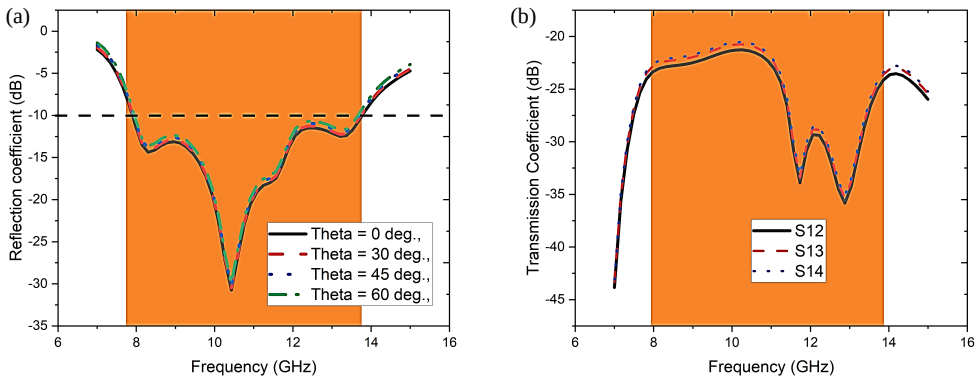

FIGURE 12. (a) Reflection coefficient, (b) transmission coefficient during conformal analysis.

7. CONFORMAL ANALYSIS

Since the proposed antenna is designed on a conformal 0.1-mm-thick polyimide substrate, a conformal analysis is conducted to evaluate its performance under bending conditions. The antenna is bent at angles of 30°, 45°, and 60°, as illustrated in Fig. 11. The corresponding S-parameters for these bending scenarios are presented in Figs. 12(a) and 12(b). The results indicate that bending the antenna at different angles does not significantly affect its impedance or isolation characteristics. Therefore, the proposed antenna demonstrates stable performance under conformal deformation and is well suited for flexible and conformal wireless applications.

Figure 13 illustrates a finite element analysis (FEA) simulation of the electromagnetic field distribution on a human hand model. The meshed structure covering the hand represents the computational domain employed for the numerical analysis. Regions of high field intensity, indicated by yellow and red colors, are primarily observed around the back of the hand, suggesting stronger electromagnetic coupling or localized resonance effects in these areas. Such simulations are essential for assessing signal propagation, electromagnetic absorption, and human-body interactions in wireless communi-

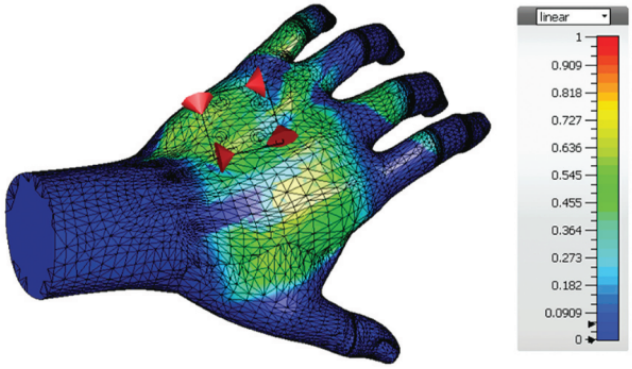

FIGURE 13. SAR analysis of the proposed antenna.

cation and biomedical applications, including RFID tracking, bio-impedance sensing, and wearable or implantable devices.

The proposed work, with compact dimensions of 22.5 mm $\times$28.8225 mm, stands out due to its higher operating frequency of 11 GHz and wide operating bandwidth spanning 7.9–13.5 GHz, making it well-suited for X-band applications, as summarized in Table 2. Compared with existing works, the proposed antenna achieves a higher gain of 4.8 dBi, outperforming several reported designs such as [31] (2.5 dBi), [38] (1 and 0.6 dBi), and [40] (0.4 and 1.6 dBi). In addition, the antenna maintains a compact electrical size of $0.023\lambda \times 0.0152\lambda$, offering superior space efficiency compared with larger designs such as [36] ($0.612\lambda \times 0.612\lambda$) while still delivering competitive performance. This combination of wide X-band coverage, enhanced gain, and compact electrical dimensions positions the proposed antenna as a strong candidate for next-generation high-frequency and wireless communication applications.

8. CONCLUSION

A compact and flexible four-port conformal MIMO antenna has been successfully designed, fabricated, and experimentally validated for wideband X-band applications. The antenna, realized on a 0.1-mm-thick polyimide substrate, demonstrates excellent electrical performance, with an impedance bandwidth extending from 7.9 to 14 GHz and inter-element isolation exceeding 20 dB. The asymmetric ground configuration combined with orthogonal element placement effectively suppresses mutual coupling while maintaining stable radiation behaviour. Both simulated and measured results confirm consistent gain ranging from 4.5 to 6 dBi, high radiation efficiency, and omnidirectional to bidirectional radiation characteristics. The extremely low envelope correlation coefficient (ECC $\approx$ 0.002), high diversity gain ($\approx$ 10 dB), and minimal channel capacity loss ($<$ 0.3 bits/s/Hz) further highlight the superior MIMO performance of the proposed design. In addition, conformal analysis demonstrates that bending angles up to 60° have a negligible impact on antenna performance, confirming its mechanical robustness and suitability for body-mounted or curved-surface integration. With a compact footprint of $0.023\lambda \times 0.0152\lambda$, the proposed antenna achieves an effective balance among miniaturization, bandwidth, and gain, making it a strong candidate for next-generation wearable, aerospace, and high-frequency X-band communication systems.

REFERENCES

[1] Yan, S. and G. A. E. Vandenbosch, "Radiation pattern-reconfigurable wearable antenna based on metamaterial structure," *IEEE Antennas and Wireless Propagation Letters*, Vol. 15, 1715–1718, 2016.

[2] Gao, G.-P., B. Hu, X.-L. Tian, Q.-L. Zhao, and B.-T. Zhang, "Experimental study of a wearable aperture-coupled patch antenna for wireless body area network," *Microwave and Optical Technology Letters*, Vol. 59, No. 4, 761–766, 2017.

[3] Van Torre, P., L. Vallozzi, C. Hertleer, H. Rogier, M. Moeneclaey, and J. Verhaevert, "Indoor off-body wireless MIMO communication with dual polarized textile antennas," *IEEE Transactions on Antennas and Propagation*, Vol. 59, No. 2, 631–642, 2011.

[4] Yan, S., P. J. Soh, and G. A. E. Vandenbosch, "Dual-band textile MIMO antenna based on substrate-integrated waveguide (SIW) technology," *IEEE Transactions on Antennas and Propagation*, Vol. 63, No. 11, 4640–4647, 2015.

[5] Xu, D., X. Tian, X. Guo, W. Jiang, W. Liu, and S. Xing, "Design and research of flexible wearable textile antenna based on GNPs/PANI/PDMS composites for 2.45 GHz," *Nanoscience and Nanotechnology Letters*, Vol. 9, No. 4, 476–480, 2017.

[6] Yamanaka, D. and M. Takahashi, "5.2 GHz band textile antenna for biological information monitoring," *IEICE Transactions on Communications*, Vol. J101-B, No. 7, 584–591, 2018.

[7] Zhu, S. and R. Langley, "Dual-band wearable textile antenna on an EBG substrate," *IEEE Transactions on Antennas and Propagation*, Vol. 57, No. 4, 926–935, 2009.

[8] Iqbal, A., A. Basir, A. Smida, N. K. Mallat, I. Elfergani, J. Rodriguez, and S. Kim, "Electromagnetic bandgap backed millimeter-wave MIMO antenna for wearable applications," *IEEE Access*, Vol. 7, 111 135–111 144, 2019.

[9] Abbasi, M. A. B., S. S. Nikolaou, M. A. Antoniades, M. N. Stevanović, and P. Vryonides, "Compact EBG-backed planar monopole for BAN wearable applications," *IEEE Transactions on Antennas and Propagation*, Vol. 65, No. 2, 453–463, 2017.

[10] Raad, H. R., A. I. Abbosh, H. M. Al-Rizzo, and D. G. Rucker, "Flexible and compact AMC based antenna for telemedicine applications," *IEEE Transactions on Antennas and Propagation*, Vol. 61, No. 2, 524–531, 2013.

[11] El Atrash, M., M. A. Abdalla, and H. M. Elhennawy, "A wearable dual-band low profile high gain low SAR antenna AMC-backed for WBAN applications," *IEEE Transactions on Antennas and Propagation*, Vol. 67, No. 10, 6378–6388, 2019.

[12] Jiang, Z. H., D. E. Brocker, P. E. Sieber, and D. H. Werner, "A compact, low-profile metasurface-enabled antenna for wearable medical body-area network devices," *IEEE Transactions on Antennas and Propagation*, Vol. 62, No. 8, 4021–4030, 2014.

[13] Chen, Y.-S. and T.-Y. Ku, "A low-profile wearable antenna using a miniature high impedance surface for smartwatch applications," *IEEE Antennas and Wireless Propagation Letters*, Vol. 15, 1144–1147, 2016.

[14] Joubert, J., J. C. Vardaxoglou, W. G. Whittow, and J. W. Odendaal, "CPW-fed cavity-backed slot radiator loaded with an AMC reflector," *IEEE Transactions on Antennas and Propagation*, Vol. 60, No. 2, 735–742, 2012.

[15] Elfergani, I., A. Iqbal, C. Zebiri, A. Basir, J. Rodriguez, M. Sajedin, A. de Oliveira Pereira, W. Mshwat, R. Abd-Alhameed, and S. Ullah, "Low-profile and closely spaced four-element MIMO antenna for wireless body area networks," *Electronics*, Vol. 9, No. 2, 258, 2020.

[16] Ling, X. and R. Li, "A novel dual-band MIMO antenna array with low mutual coupling for portable wireless devices," *IEEE Antennas and Wireless Propagation Letters*, Vol. 10, 1039–1042, 2011.

[17] Gupta, A., A. Kansal, and P. Chawla, "Design of a wearable MIMO antenna deployed with an inverted U-shaped ground stub for diversity performance enhancement," *International Journal of Microwave and Wireless Technologies*, Vol. 13, No. 1, 76–86, 2021.

[18] Shamsuri Agus, A. N. S., T. Sabapathy, M. Jusoh, M. A. Abdelghany, K. Hossain, S. Padmanathan, S. S. Al-Bawri, and P. J. Soh, "Combined RIS and EBG surfaces inspired meta-wearable textile MIMO antenna using viscose-wool felt," *Polymers*, Vol. 14, No. 10, 1989, 2022.

[19] Lu, X., S. Venkatesh, H. Saeidi, and K. Sengupta, "Integrated intelligent electromagnetic radiator design for future THz communication: A review," *Chinese Journal of Electronics*, Vol. 31, No. 3, 499–515, 2022.

[20] Kumar Biswas, A. and U. Chakraborty, "Compact wearable MIMO antenna with improved port isolation for ultra-wideband applications," *IET Microwaves, Antennas & Propagation*, Vol. 13, No. 4, 498–504, 2019.

[21] Wen, D., Y. Hao, M. O. Munoz, H. Wang, and H. Zhou, "A compact and low-profile MIMO antenna using a miniature circular high-impedance surface for wearable applications," *IEEE Transactions on Antennas and Propagation*, Vol. 66, No. 1, 96–104, 2018.

[22] Biswas, A. K. and U. Chakraborty, "A compact wide band textile MIMO antenna with very low mutual coupling for wearable applications," *International Journal of RF and Microwave Computer-Aided Engineering*, Vol. 29, No. 8, e21769, 2019.

[23] Roy, S., S. Ghosh, S. S. Pattanayak, and U. Chakarborty, "Dual-polarized textile-based two/four element MIMO antenna with improved isolation for dual wideband application," *International Journal of RF and Microwave Computer-Aided Engineering*, Vol. 30, No. 9, e22292, 2020.

[24] Biswas, A. K. and U. Chakraborty, "Reconfigurable wide band wearable multiple input multiple output antenna with hanging resonator," *Microwave and Optical Technology Letters*, Vol. 62, No. 3, 1352–1359, 2020.

[25] Liu, F., J. Guo, L. Zhao, G.-L. Huang, Y. Li, and Y. Yin, "Dual-band metasurface-based decoupling method for two closely packed dual-band antennas," *IEEE Transactions on Antennas and Propagation*, Vol. 68, No. 1, 552–557, 2020.

[26] Liu, F., J. Guo, L. Zhao, G.-L. Huang, Y. Li, and Y. Yin, "Ceramic superstrate-based decoupling method for two closely packed antennas with cross-polarization suppression," *IEEE Transactions on Antennas and Propagation*, Vol. 69, No. 3, 1751–1756, 2021.

[27] Li, H., S. Sun, B. Wang, and F. Wu, "Design of compact single-layer textile MIMO antenna for wearable applications," *IEEE Transactions on Antennas and Propagation*, Vol. 66, No. 6, 3136–3141, 2018.

[28] Iqbal, A., A. Smida, A. J. Alazemi, M. I. Waly, N. K. Mallat, and S. Kim, "Wideband circularly polarized MIMO antenna for high data wearable biotelemetric devices," *IEEE Access*, Vol. 8, 17 935–17 944, 2020.

[29] Li, W., Y. Hei, P. M. Grubb, X. Shi, and R. T. Chen, "Compact inkjet-printed flexible MIMO antenna for UWB applications," *IEEE Access*, Vol. 6, 50 290–50 298, 2018.

[30] Bell, A. J., R. Fossi, and C. Petrucci, "Calculations of dielectric properties from the superparaelectric model of relaxors," *Journal of Physics: Condensed Matter*, Vol. 5, No. 46, 8773, 1993.

[31] Kulkarni, J., C.-Y.-D. Sim, A. K. Poddar, U. L. Rohde, and A. G. Alharbi, "A compact circularly polarized rotated L-shaped antenna with J-shaped defected ground strucutre for WLAN and V2X applications," *Progress In Electromagnetics Research Letters*, Vol. 102, 135–143, 2022.

[32] Kulkarni, J., C.-Y.-D. Sim, B. Garner, and Y. Li, "A dual-CP quad-port MIMO antenna with reduced mutual coupling for X-band application," *IEEE Antennas and Wireless Propagation Letters*, Vol. 22, No. 9, 2085–2089, 2023.

[33] Elwi, T. A. and A. M. Al-Saegh, "Further realization of a flexible metamaterial-based antenna on indium nickel oxide polymerized palm fiber substrates for RF energy harvesting," *International Journal of Microwave and Wireless Technologies*, Vol. 13, No. 1, 67–75, 2021.

[34] Haque, S. M. and H. Alam, "Miniaturized dual-band slot antenna design for GPS, amateur radio and WLAN applications," *International Journal of RF and Microwave Computer-Aided Engineering*, Vol. 30, No. 4, e22125, 2020.

[35] Kulkarni, J. S. and C.-Y. D. Sim, "Low-profile, multiband & wideband 'C-Shaped' monopole antenna for 5G and WLAN applications," in *2020 International Conference on Radar, Antenna, Microwave, Electronics, and Telecommunications (ICRAMET)*, 366–371, Tangerang, Indonesia, 2020.

[36] Kulkarni, N. P., N. B. Bahadure, P. D. Patil, and J. S. Kulkarni, "Flexible interconnected 4-port MIMO antenna for sub-6 GHz 5G and X band applications," *AEU — International Journal of Electronics and Communications*, Vol. 152, 154243, 2022.

[37] Al-Khaylani, H. H., T. A. Elwi, and A. A. Ibrahim, "A novel miniaturized reconfigurable microstrip antenna based printed metamaterial circuitries for 5G applications," *Progress In Electromagnetics Research C*, Vol. 120, 1–10, 2022.

[38] Patel, R. and T. K. Upadhyaya, "Compact planar dual band antenna for WLAN application," *Progress In Electromagnetics Research Letters*, Vol. 70, 89–97, 2017.

[39] Sura, P. R. and M. Sekhar, "Circularly polarized dual band dual slot antenna for WLAN, Wi-MAX and Wi-Fi applications," *IETE Journal of Research*, Vol. 69, No. 3, 1550–1555, 2023.

[40] Ali, M. S. M., S. K. A. Rahim, M. I. Sabran, M. Abedian, A. Eteng, and M. T. Islam, "Dual band miniaturized microstrip slot antenna for WLAN applications," *Microwave and Optical Technology Letters*, Vol. 58, No. 6, 1358–1362, 2016.

[41] Elwi, T. A., D. A. Jassim, and H. H. Mohammed, "Novel miniaturized folded UWB microstrip antenna-based metamaterial for RF energy harvesting," *International Journal of Communication Systems*, Vol. 33, No. 6, e4305, 2020.

[42] Joshi, R., E. F. N. M. Hussin, P. J. Soh, M. F. Jamlos, H. Lago, A. A. Al-Hadi, and S. K. Podilchak, "Dual-band, dual-sense textile antenna with AMC backing for localization using GPS and WBAN/WLAN," *IEEE Access*, Vol. 8, 89 468–89 478, 2020.

[43] Bag, B., P. Biswas, R. Mondal, S. Biswas, and P. P. Sarkar, "Dual-band dual-sense circularly polarized U-and L-shaped strip monopole antenna for WiMAX/WLAN applications," *Journal of Electromagnetic Waves and Applications*, Vol. 33, No. 18, 2434–2448, 2019.

[44] Gowrish, B. and A. Basu, "Analysis and design of a dual-band stepped impedance PCB monopole antenna," *IETE Journal of Education*, Vol. 58, No. 1, 29–38, 2017.

[45] Blanch, S., J. Romeu, and I. Corbella, "Exact representation of antenna system diversity performance from input parameter description," *Electronics Letters*, Vol. 39, No. 9, 705–707, 2003.

[46] Agarwal, S. and U. Raque, "A small-scaled super wideband circular ring fractal antenna with high BDR for SHF applications," *Progress In Electromagnetics Research C*, Vol. 134, 53–63, 2023.

[47] Talukder, M. S., M. M. Alam, M. T. Islam, M. Moniruzzaman, R. Azim, A. G. Alharbi, A. I. Khan, M. Moinuddin, and M. Samsuzzaman, "Rectangular slot with inner circular ring patch and partial ground plane based broadband monopole low SAR patch antenna for head imaging applications," *Chinese Journal of Physics*, Vol. 77, 250–268, 2022.

[48] Saurabh, A. K., P. S. Rathore, and M. K. Meshram, "Compact wideband four-element mimo antenna with high isolation," *Electronics Letters*, Vol. 56, No. 3, 117–119, 2020.

[49] Jhunjhunwala, V. K., P. Kumar, A. P. Parameswaran, P. R. Mane, O. P. Kumar, T. Ali, S. Pathan, S. Vincent, and a. P. Kumar, "A four port flexible uwb mimo antenna with enhanced isolation for wearable applications," *RINENG*, Vol. 24, 103147, 2024.